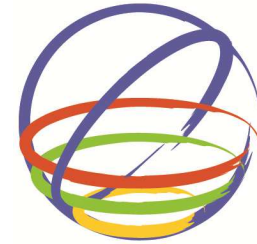


# Unbonded Prestressed Columns for Earthquake Resistance

A.S. Larkin, D.H. Sanders & M.S. Saïdi

University of Nevada Reno, Nevada



15 WCEE  
LISBOA 2012

## SUMMARY:

Modern structures are able to withstand significant shaking caused by earthquakes. By implementing unbonded post-tensioned tendons in bridge column, the damage can be significantly lower than that of a standard reinforced concrete column. Two unbonded post-tensioned columns were tested to evaluate their seismic performance. The columns were identical except for the amount of longitudinal reinforcement crossing the column/footing interface. The main objective of the research was to investigate modified tendon details, the effect of the longitudinal reinforcement ratio on re-centering capabilities, and the initial post-tensioning force that will not yield the tendons at large drift ratios. Each column was tested in a cyclic pattern to evaluate their performance.

*Keywords: Unbonded post-tensioning; bridge; re-centering; earthquake resistance*

## 1. INTRODUCTION

The number one concern with seismic engineering design is to sustain life safety. Once a structure can sustain life safety through an earthquake, the next step is to minimize the amount of damage to the affected structure. Minimizing the amount of damage will allow for speedy repairs and a reduction in closure time. For bridge columns, the introduction of unbonded post-tensioned tendons reduces the amount of residual displacement following large lateral drifts, and in turn reduces damage and closure time. To further investigate the benefits of unbonded post-tensioning, two columns were tested.

The presented research is based on a prototype column of 1524 mm-diameter. For full-scale columns of this size, the amount of post-tensioning that would be required to promote re-centering would be around 10% of  $f'_c A_g$ . Typically, the initial stress in the tendon is between 20% and 30% of  $f_{pu}$ . Therefore, if the prototype column was constructed with 31 MPa concrete, and 15 mm diameter strands are used, a total of between 72 and 109 strands would be required. While this number is not only too large for one tendon, providing multiple tendons will maintain post-tensioning while a tendon is being replaced and permit the tendons to exit from the side of the footing in a symmetrical manner. The columns tested were 0.4-scale models of a 1524 mm-diameter column, resulting in 610 mm-diameter models. To evenly distribute the post-tensioning force required for re-centering, four tendons, each with four 15 mm 1860 MPa 7-wire strands were evenly spaced at 137.2 mm (22.5% of column diameter) around the center of the column cross section.

Following a major earthquake, it is highly likely that bridge columns have undergone large lateral displacements. Post-tensioned columns are designed to not have any yielding or damage of the tendons. However, following a major seismic event it is essential to have the ability to inspect and replace the tendons if necessary. Previous tests have utilized straight tendon or bar that is anchored in the base of the footing. This makes it very difficult to replace the tendons. By anchoring the tendons in the side of the footing, it makes it possible to remove the tendons. For the specimens tested in this experiment, all four tendons were anchored in the side of the footing (see Figure 1).

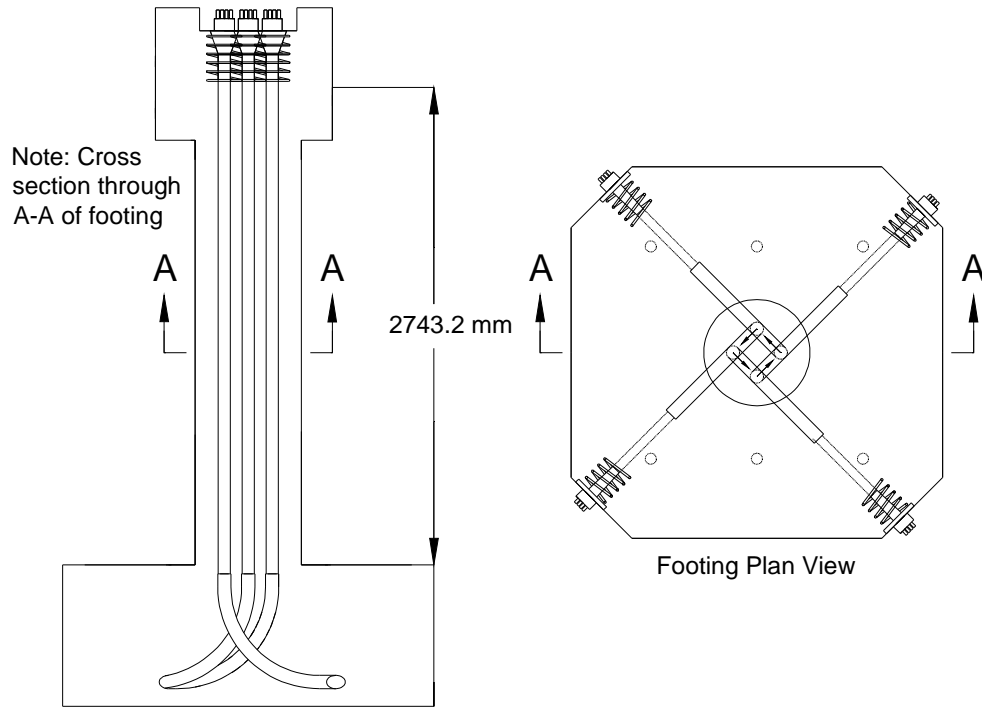


**Figure 1: Tendons Anchored in Corners of Footing**

## 2. LITERATURE REVIEW

Many researchers in the past have implemented the use of unbonded post-tensioned tendons in column design. The primary focus of prior research was to investigate the magnitude of the re-centering effects. To focus on the magnitude of the re-centering effects, most columns had a small longitudinal reinforcement ratio that crossed the joint between the column base and the footing, and some columns did not have any longitudinal reinforcement crossing this joint.

Segmental unbonded post-tensioned columns were constructed with no longitudinal reinforcement crossing the joint between the base of the column and the footing, except for a single tendon. The single tendon was centrally located and anchored in the base of the footing. By utilizing unbonded tendons, inelastic straining of the tendon did not occur and the initial prestress force was maintained throughout the testing (Hewes and Priestley, 2002). While this configuration showed excellent re-centering capabilities with negligible residual displacements, there was no longitudinal connectivity between the column and footing in case of a tendon failure, and in turn limited energy dissipation.

Partially prestressed columns were evaluated by Jeong et al.. Several specimens were tested, each being lightly reinforced in the longitudinal direction. The models varied from having unbonded mild reinforcement crossing the joint between the column base and footing, to one specimen having a steel jacket surrounding the base of the column in the plastic hinge region for added seismic protection. The initial prestress force for the specimens also varied between 5% and 9% of  $f'_c A_g$ . The tendon remained elastic during all of the tests, indicating that a safe initial prestress force had been selected (Jeong, et al., 2008). The single tendon centrally located in the column cross section was anchored in the base of the footing in each specimen.

Research conducted by Ou et al., 2009, focused on square segmental hollow core unbonded post-tensioned columns. The four columns tested had a longitudinal reinforcement ratio varying from 0% to

1%. The specimens with mild longitudinal reinforcement crossing the joint between the column base and the footing were unbonded to avoid premature failure from low cycle fatigue. Following testing, the column without any longitudinal reinforcement crossing the joint between the base of the column and footing displayed drift capacities of 4.6%, while the columns with mild reinforcement displayed drifts of 5%. Each of the four columns contained four post-tensioned tendons that were located within the hollow core and anchored in the base of the footing (Ou et al., 2009).

### 3. MOTIVATION

Based on the literature review, it was noted that there are several parameters that require more investigation. Much of the previous research investigates re-centering capabilities of unbonded post-tensioned columns with very little to no longitudinal reinforcement crossing the column/footing interface. Reinforcement ratios greater than 1.0% should be tested to gain a better perspective of the effect of the reinforcement on re-centering. Developing tendon details requires further investigation to develop a realistic full-scale configuration. Prestress area and initial force has been tested with a wide range of values without a definite value for the best all-around column performance. Not only should re-centering be further investigated, but tendon strains at large lateral displacements, even beyond column failure should also be looked at. Axial dead load has been investigated at a wide range of values, as this can vary greatly in modern bridge design. Further research on the axial load should be investigated to provide the best all-around column performance, and an accurate unbonded post-tensioned analytical model is required for further investigation, since only a few columns can be tested in each project.

### 4. DESIGN OF SPECIMENS AND TEST SETUP

The two columns selected for testing were initially targeted to have identical properties except for the amount of longitudinal reinforcement crossing the joint between the column base and footing. Achieving identical forces in the tendons between the two specimens was difficult and ended with a slight variation between the initial post-tensioning forces (% of  $f'_c A_g$ ). The column parameters and cross sections are shown in Table 1 and Figure 2, respectively. The tested material properties for each column are shown in Tables 2 and 3.

**Table 1:** Column Parameters

| Column | $\rho_l$ | $\rho_s$ | PT (initial)             | Dead Load              | Height    | Diameter | Aspect Ratio |
|--------|----------|----------|--------------------------|------------------------|-----------|----------|--------------|
| PT-LL  | 0.69%    | 1.00%    | 7.7% $f_c A_g$<br>698 kN | 6% $f_c A_g$<br>543 kN | 2743.2 mm | 609.6 mm | 4.5          |
| PT-HL  | 1.33%    | 1.00%    | 9.6% $f_c A_g$<br>868 kN | 6% $f_c A_g$<br>543 kN | 2743.2 mm | 609.6 mm | 4.5          |



**Figure 2:** Column Cross Sections

**Table 2:** Concrete Properties

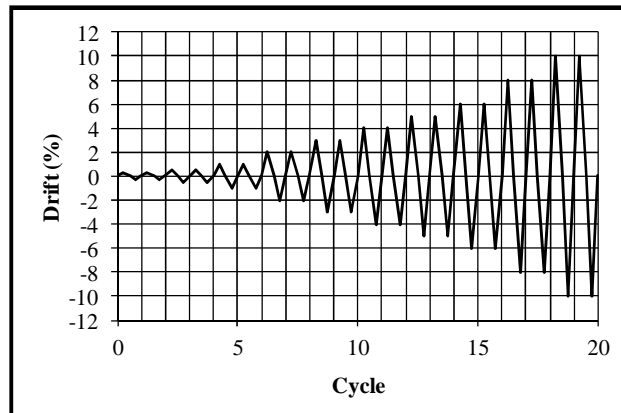
| Column | Segment              | 7-Day Strength, MPa | Test Day, MPa |
|--------|----------------------|---------------------|---------------|
| PT-LL  | Footing              | 30.1                | 37.1          |
|        | Column & Column Head | 23.3                | 29.9          |
| PT-HL  | Footing              | 30.1                | 37.9          |
|        | Column & Column Head | 23.3                | 31.5          |

**Table 3:** Steel Properties

| Tested Bar                   | $f_y$ , MPa | $f_u$ , MPa |
|------------------------------|-------------|-------------|
| Transverse Bars: #3          | 492         | 652         |
| Longitudinal Bars: #5        | 495         | 666         |
| Longitudinal Bars: #7        | 481         | 774         |
| Post-Tensioned Strand: 15 mm | 1,703       | 1,937       |

The tendons were stressed once the concrete had reached 28 day strength. In order to properly seat the wedges, the tendons were stressed to 75% of  $f_{pu}$ . This high level of stress is well above the initial stress limit for testing. In order to account for the high level of stress needed to seat the wedges, steel shims were placed beneath the anchor heads prior to stressing. Once all of the strands had been individually stressed, a monostrand jack was used to perform a “lift-off.” Once the anchor head had been lifted off the shim stack, steel shims could then be removed until the desired stress level was achieved.

The test setup for each specimen consisted of a strong floor, reaction wall, and 979-kN actuator to produce the loading protocol shown in Figure 3. Before the column was placed in position on the strong floor, four 50.8 mm by 101.6 mm wood blocks were placed underneath the footing to allow for the placement of high strength grout. The grout allows for an even and level surface for the footing to rest on. The column footing was then secured to the 914.4 mm deep strong floor using six 31.75 mm post-tensioned bars. Each of the six post-tensioned bars had a 444.8 kN force applied to insure that the footing would not slide or rock during testing. The reaction wall was made by stacking two columns of three 1219 x 1219 x 2438 mm concrete blocks, with one additional block added to the top of the stack nearest the column to achieve the proper height for the actuator to meet the column head. The reaction wall was also secured to the strong floor with 31.75 mm post-tensioned bars, with each bar having a 444.8 kN force applied. The test setup is shown in Figure 4.

**Figure 3:** Loading Protocol



**Figure 4: Test Setup**

A steel spreader beam was bolted to the top of each column and was used to distribute the axial dead load to the column. The spreader beam was 1219 mm in length, leaving an overhang on each side of the column head. Two hydraulic rams were then placed on the spreader beam overhangs. Two high strength 31.75 mm threaded rods ran through the hydraulic rams, load cell, footing, and were anchored against the base of the strong floor to apply the axial dead load. The axial dead load was maintained throughout the testing sequence through an accumulator which held the axial load constant and equal in each of the hydraulic rams.

## 5. RESULTS

From the cyclic loading applied to each column, a lateral force and displacement hysteresis curve was produced. Each hysteresis curve was broken up into the push cycle (positive), and the pull cycle (negative). The absolute values from the negative envelope were then taken and superimposed on the positive envelope and an average pushover envelope was taken between these two envelopes. This average curve was then considered the pushover curve for the column. The pushover curves for column PT-LL and PT-HL are shown in Figures 5 and 6, respectively. In each curve, the “X” indicates the location of the first longitudinal reinforcing bar fracture.

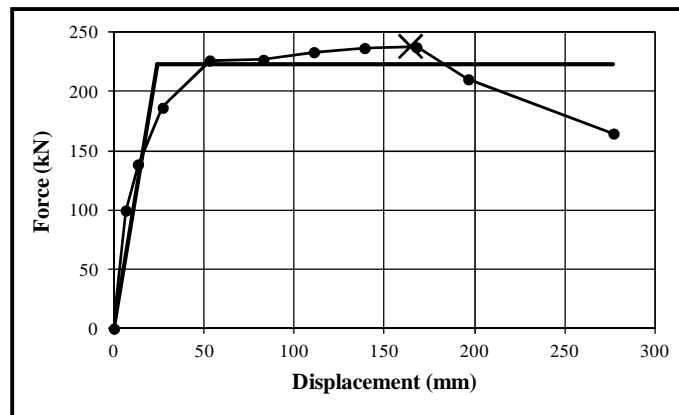


**Figure 5: PT-LL Average Pushover Curve**

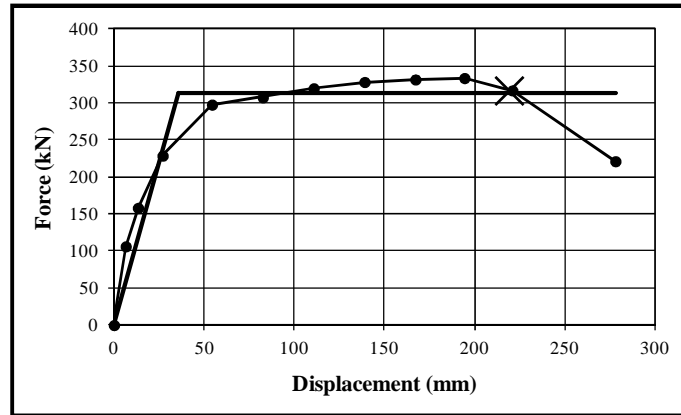


**Figure 6:** PT-HL Average Pushover Curve

The first bar yield displacement was determined by the column displacement when the first longitudinal rebar yielded. This value was then used to plot a straight line on the pushover curve, beginning at zero force and zero displacement. A straight horizontal line was then plotted near the top of the pushover curve, where the area under the straight horizontal line bounded by the pushover curve was equal to the area under the pushover curve bounded by the straight horizontal line. The point where the two straight lines intersect is the effective yield displacement. Two different ductility displacements were then defined. The first is termed the “ductility displacement capacity” and is defined as the ultimate displacement (ultimate displacement was defined as displacement at 80% of the peak lateral force in the column) divided by the effective yield displacement. The second is termed “ductility at first fracture” and is defined as the column displacement when the first longitudinal rebar fractures divided by the effective yield displacement. Column PT-LL had a first bar yield displacement of 16.5 mm, leading to an effective yield displacement of 24.1 mm. The ultimate displacement was 231.1 mm at a drift of 8.4% leading to ductility displacement capacity of 9.6. The displacement at first fracture was 167.6 mm at a drift of 6.1% leading to ductility at first fracture of 6.9. Column PT-HL had a first bar yield displacement of 25.9 mm, leading to an effective yield displacement of 36.1 mm. The ultimate displacement was 250.7 mm at a drift of 9.1% leading to ductility displacement capacity of 7.0. The displacement at first fracture was 217.4 mm at a drift of 7.9% leading to ductility at first fracture of 6.0.

The four tendons in each column consisted of four 15 mm 1860 MPa 7-wire strands. The tendons were numbered one through four, with tendons two and four located on the axis of column rotation, and tendons one and three located on the extreme ends. Throughout testing, tendons one and three had the largest strains of the four tendons. The initial tendons force was carefully selected and kept within the lower elastic region so the tendons would not yield or fracture under large lateral displacements. Figures 7 and 8 show the microstrain in tendons one and four of PT-LL with respect to the lateral drift of the column. In each figure, negative microstrain represents tension. The two tendons (one and three) on the outside of the axis of rotation felt the largest strains, shown in Figure 7. The tendons (two and four) that were on the same axis of column rotation, felt significantly less strain as shown in Figure 8. The tendons do not begin to yield until a microstrain of at least 8600 is reached. It can be seen that even the tendons located on the extreme ends, such as tendon one, do not begin to reach their yield strains, even at large drift ratios. Column PT-HL behaved very similarly to column PT-LL and did not reach a strain of more than 6500 microstrain, even at drift levels as high as 10%. The columns were pushed to 10% drift, even though they had failed, to study the impact of large displacements on tendon stresses.

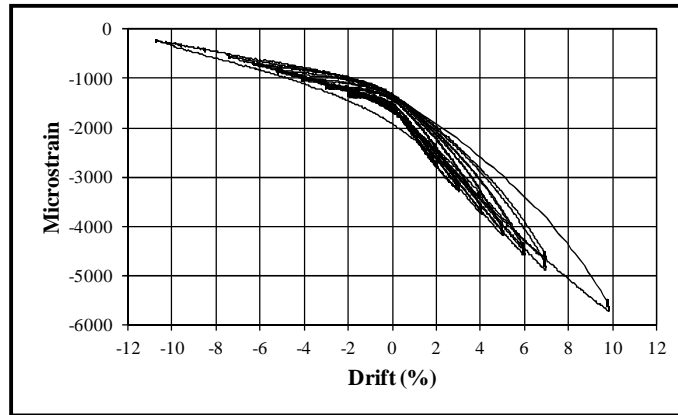


**Figure 7:** PT-LL Microstrain in Tendon 1

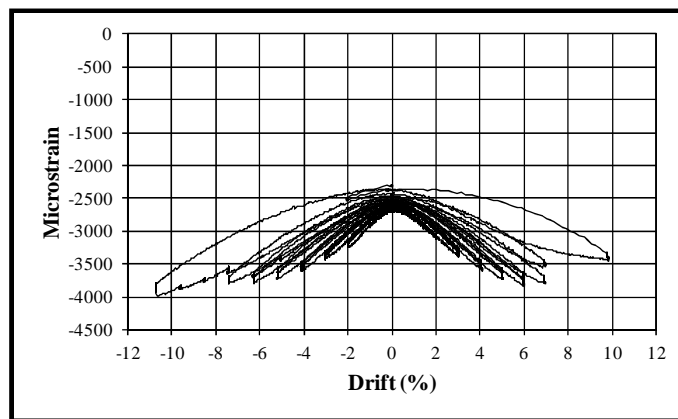


**Figure 8:** PT-LL Microstrain in Tendon 4

Figure 9 shows the full hysteresis curve for column PT-LL. Following construction, the cover concrete was found to be 25.4 mm on one side of the column, and 50.8 mm on the other side. Uneven concrete cover resulted in a shifted column core, so the core location was not at the true center of the column. This offset caused residual displacements and peak loads to differ from the push and pull cycles. Figure 9 shows the re-centering capabilities provided by the post-tensioning, leading to small residual displacements in the column. At a drift level of 6%, column PT-LL had a residual displacement on the positive side of the hysteresis curve of 39.9 mm and a residual displacement on the negative side of the hysteresis curve of 87.6 mm, resulting in an average residual displacement of 63.8 mm. The full hysteresis curve for column PT-HL is shown in Figure 10. The residual displacements are larger than PT-LL due to the increase in amount of longitudinal reinforcement. At a drift level of 6%, column PT-HL had a residual displacement on the positive side of the hysteresis curve of 79.2 mm and a residual displacement on the negative side of the hysteresis curve of 84.1 mm resulting in an average residual displacement of 81.7 mm.

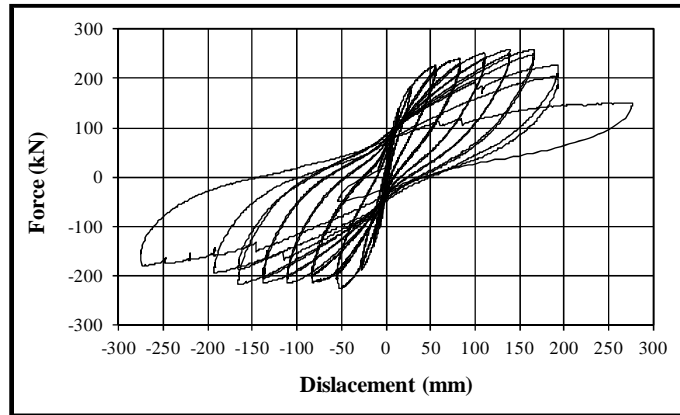


**Figure 9: PT-LL Hysteresis**

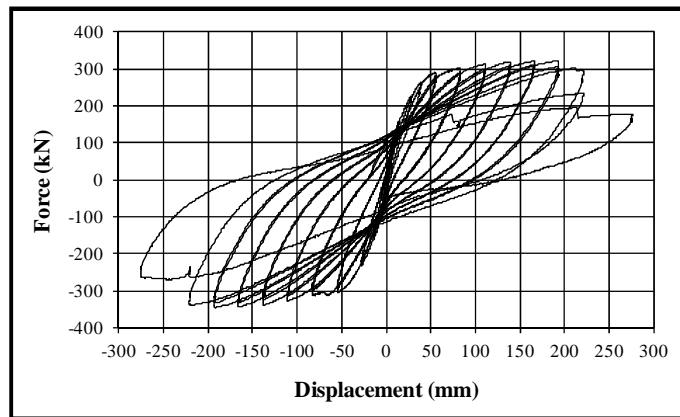


**Figure 10: PT-HL Hysteresis**

Once all testing was complete, it was important to remove one of the extreme tendons to determine how much damage was caused by the extreme curve in the footing that each tendon passed through. Since column PT-HL was initially stressed slightly higher than column PT-LL, it was decided to extract one of the extreme tendons from PT-HL for inspection. Figure 11 and 12 show the removed tendon. As the figures show, there is very minimal damage, even after eight cycles of 4% drift or greater. Since there was very minor damage in only one tendon, the encapsulated greased strands will be able to resist corrosion very well.



**Figure 11: Removed Tendon (After Testing)**



**Figure 12:** Removed Tendon at Bend in Location (After Testing)

## 6. PARAMETRIC STUDY

A parametric study was conducted using the prototype column to determine the full-scale behavior. The basic geometric properties of the two columns, PT-LL and PT-HL, were used as the basis for this study. The same loading protocol as the scaled models was used to investigate the pushover response, hysteretic behavior, residual displacements, and tendon stresses at various drift levels. An initial base model was created to make comparisons with the scaled results, which provided a close correlation. A parametric study was then conducted, investigating changes in; axial load from 6%  $f'_c A_g$  up to 10%, 15%, and 20% of  $f'_c A_g$ , initial post-tensioning force were increased from 10%  $f'_c A_g$  up to 15% and 20%  $f'_c A_g$ , concrete strength was increased from 31 MPa to 69 MPa, and the tendon location was increased from 22.5% of the column diameter out to 30% of the column diameter.

Based on observations from the parametric study, the axial dead load and initial post-tensioning force should be set at 6% and 10% of  $f'_c A_g$ , respectively, the values of the original prototype columns. Increasing the amount of axial dead load and initial post-tensioning force resulted in columns with less cyclic capacity, lower column displacements at peak lateral force, and increased residual displacements from the overall results looking at all drift levels. While considering the concrete strength in determining the axial load and initial post-tensioning based on  $f'_c A_g$ , a concrete strength of 31 MPa should be used. The actual concrete strength for the column construction can be increased, up to 69 MPa to improve overall performance, based on the results of the parametric study. Although column performance was not checked with a concrete strength between 31 MPa and 69 MPa, it is assumed that a concrete strength between these values will produce reasonable results, and continue to improve results as the strength is increased from 31 MPa to 69 MPa. Increasing the distance out from the center of the column cross section to the tendons from 22.5% to 30% of the column diameter showed a slight improvement on residual displacements, but resulted in a large increase in tendon stresses, bringing them very close to the yield stress at 8% drift. Therefore, the tendon location should remain at 22.5% of the column diameter.

## 7. CONCLUSIONS

Constructing each column with four separate tendons centrally located within the column cross section provided sufficient area and spacing for the tendons in the experimental specimens. The area and spacing of tendons would also work in a full-scale design. Exiting the tendons out of the corners of the footing provided the possibility of removing the tendons, and did not display any negative effects. Encapsulating the tendons in greased sleeves provided corrosion protection and held up well with minimal damage following many cycles at large drift ratios.

Selecting an initial tendon force of 10% of  $f'_c A_g$ , and an initial tendon stress of 21% of  $f_{pu}$ , provided re-centering capabilities and did not yield the tendons. Once the columns reached failure (8.4% drift for PT-LL, and 9.1% drift for PT-HL at 80% of maximum load), they were pushed to a drift ratio of 10% (274 mm of displacement) to measure the tendon stresses. At a large drift ratio of 10%, the tendon stresses remained below the yield stress, with a maximum stress of 1041 MPa for column PT-LL, and 1165 MPa for column PT-HL. The yield stress of the tendons was 1703 MPa, and 70% of the yield stress (a good target to stay below) was 1192 MPa. These maximum stresses were measured in the tendons located on the extreme sides of the column, where the highest tendon stresses were measured.

Using unbonded tendons in each column helped minimize residual displacements. Column PT-LL showed an average residual displacement between the positive and negative sides of the hysteresis response of 8.0 mm at a drift ratio of 2% (54.9 mm). At larger drift ratios, the residual displacement remained low, with measured residual displacements of 47.0 mm at 5% drift (137 mm), 63.6 mm at 6% drift (165 mm), and 74.6 mm at 7% drift (192 mm). These residual displacements corresponded to 34.3% of the maximum lateral drift at 5% drift (137 mm), 38.6% of the maximum lateral drift at 6% drift (165 mm), and 38.9% of the maximum lateral drift at 7% drift (192 mm). Column PT-HL showed an average residual displacement between the positive and negative sides of the hysteresis response of 7.7 mm at a drift of 2% (54.9 mm). At larger drift ratios, the residual displacement increased beyond the values of column PT-LL, with measured residual displacements of 57.4 mm at 5% drift (137 mm), 77.9 mm at 6% drift (165 mm), and 100.0 mm at 7% drift (192 mm). These residual displacements corresponded to 41.9% of the maximum lateral drift at 5% drift (137 mm), 47.4% of the maximum lateral drift at 6% drift (165 mm), and 52.1% of the maximum lateral drift at 7% drift (192 mm). Note the lower residual displacements of column PT-LL compared to column PT-HL. The longitudinal reinforcement ratio had a large impact on the column re-centering capabilities, and the lower reinforcement ratio resulted in significantly smaller residual displacements.

#### ACKNOWLEDGMENT

Support for this research was provided by the Nevada Department of Transportation. The results presented within are of interpretation of the authors and do not necessarily represent the opinion of the sponsoring organization.

#### REFERNECES

- Hewes, J. T., and Priestley, M. J. N. (2002). "Seismic Design and Performance of Precast Concrete Segmental Bridge Columns." Structural Systems Research Project, *Rep. No. SSRP-2001/25*, University of California, San Diego, La Jolla, California.
- Jeong, H. I., Sakai, J., and Mahin, S. A. (2008). "Shaking Table Tests and Numerical Investigation of Self-Centering Reinforced Concrete Bridge Columns." Pacific Earthquake Engineering Research Center, *Rep. No. PEER 2008/06*, University of California, Berkeley, Berkeley, California.
- Ou, Y., Wang, P. H., Tsai, M.-C., Chang, K.-C., and Lee, G. C. (2009). "Large-scale experimental study of precast segmental unbonded post-tensioned concrete bridge columns for seismic regions." *Journal of Structural Engineering, ASCE*